Journal of Coordination Chemistry
Publication details, including instructions for authors and subscription information:
http://www.tandfonline.com/loi/gcoo20

Synthesis, structure, and catalytic bromination of supramolecular oxovanadium complexes containing oxalate

Chen Chen [a], Feng-Ying Bai [b], Rui Zhang [a], Ge Song [a], Hui Shan [a], Na Xing [a] & Yong-Heng Xing [a]

[a] College of Chemistry and Chemical Engineering, Liaoning Normal University, Dalian, P.R. China

[b] College of Life Science, Liaoning Normal University, Dalian, P.R.China

Accepted author version posted online: 17 Jan 2013.Published online: 05 Mar 2013.

To cite this article: Chen Chen, Feng-Ying Bai, Rui Zhang, Ge Song, Hui Shan, Na Xing & Yong-Heng Xing (2013) Synthesis, structure, and catalytic bromination of supramolecular oxovanadium complexes containing oxalate, Journal of Coordination Chemistry, 66:4, 671-688, DOI: 10.1080/00958972.2013.765561

To link to this article: http://dx.doi.org/10.1080/00958972.2013.765561

Journal of Coordination Chemistry
Vol. 66, No. 4, 20 February 2013, 671–688

Synthesis, structure, and catalytic bromination of supramolecular oxovanadium complexes containing oxalate

CHEN CHEN†, FENG-YING BAI‡, RUI ZHANG†, GE SONG†, HUI SHAN†, NA XING† and YONG-HENG XING*†

†College of Chemistry and Chemical Engineering, Liaoning Normal University, Dalian, P.R. China
‡College of Life Science, Liaoning Normal University, Dalian, P.R. China

(*Received 31 August 2012; in final form 2 November 2012*)

Three supramolecular complexes, $[VO(phen)(C_2O_4)(H_2O)]\cdot CH_3OH$ (**1**) $[(VO)_2(u_2\text{-}C_2O_4)(C_2O_4)_2(H_2O)_2]\cdot L\cdot H_2O$ (**2**), and $[(4,4'\text{-bipyH}_2)_{0.5}]^+[VO_2(2,6\text{-dipic})]^-\cdot 2H_2O$ (**3**) (phen = 1,10-phenanthroline 4,4′-bipy = 4,4′-bipyridine, 2,6-dipic = 2,6-pyridinedicarboxylic, L = 1,4-bis((3,5-dimethyl-1*H*-pyrazol-1-yl)methyl)benzene), have been prepared and characterized by elemental analysis, IR, and UV–vis spectroscopy and single-crystal diffraction analysis. Structural analysis shows that the three complexes all contain carboxylate and V=O moiety; vanadium of **1** and **2** are six coordinate with distorted octahedral geometry with N_2O_4 and O_6 donor sets, respectively, while **3** is five coordinate with distorted trigonal bipyramidal geometry with a NO_4 donor set. The complexes exhibit catalytic bromination activity in the single-pot reaction for the conversion of phenol red to bromophenol blue in H_2O–DMF at 30 ± 0.5 °C with pH 5.8, indicating that they can be considered as functional model vanadium-dependent haloperoxidases. In addition, electrochemical behaviors are also studied.

Keywords: Vanadium complex; Hydrogen bonds; Electrochemistry; Bromination reaction activity

1. Introduction

Coordination chemistry of vanadium has received attention because of the biological and catalytic properties of relevant systems [1–8], such as haloperoxidation, nitrogen fixation [9,10], phosphorylation, glycogen metabolism, and insulin mimicking [11–13]. In particular, vanadate-dependent haloperoxidases (V-HPOs) have developed in catalyzing different oxidation reactions like oxidation of halides [14,15], which could catalyze the two-electron oxidation of halides to an $\{X^+\}$ species, where $\{X^+\}$ is X_2, X_3^- and/or XOH, that is, hypohalous acid in the presence of hydrogen peroxide, resulting in halogenation of certain organic substrates [16].

Structural characterization of vanadium-dependent haloperoxidases has revealed that vanadium is covalently linked to the N^{ε} of imidazolyl of a histidine, and further through extensive hydrogen bonding to a variety of amino acid side chains (Arg, His, Ser, Lys) and interstitial water in the proximity of the active centre [17,18]. Bromoperoxidation was

*Corresponding author. Email: xingyongheng@lnnu.edu.cn

Journal of Coordination Chemistry
ISSN 0095-8972 print/ISSN 1029-0389 online
http://dx.doi.org/10.1080/00958972.2013.765561

influenced by interactions of covalents and also affected by non-covalent interactions [19], such as hydrogen-bonding and metal-ligand coordination, as well as π-π stacking, hydrophobic, ionic, and van der Waals forces [20,21]. The role of hydrogen bonding in stabilization of structures as well as in the functions of various metalloproteins is well known in biochemistry [22]. Hydrogen-bonding interactions influence catalytic reactions to some extent.

Numerous supramolecular vanadium complexes containing N, O-donor ligands (as acceptors for participating in inter- and intramolecular hydrogen bonds) have been prepared [23,24], such as (i) [VO(OMe)(tbhsR)] (H_2tbhsR: the O, N, S-donor Schiff bases derived from thiobenzhydrazide and 5-substituted salicylaldehydes; R = H, OMe, Cl, Br and NO_2) [25], which form dimeric, 1-D and 2-D self-assembled structures via intermolecular C–H···O and O–H···O interactions. (ii) [$VO(L)_2$] (L = N-salicylidin-2-bromoethylimine), which form a zigzag chain via only two intermolecular hydrogen bonds (C–H···O) [26]. However, study on these complexes in catalytic reactions of bromoperoxidation is comparatively rare. Our group has a long-standing interest in investigation of the influence of oxovanadium complexes containing N, O-donors (especially carboxylates) on bromoperoxidation. We have reported a family of crystal structures of oxovanadium complexes with carboxylate ligands: $TpVO(L_1)$ and $Tp^*VO(pzH^*)(L_2)$ (Tp = hydrotris(pyrazolyl)borate, HL_1 = 5-methyl-1*H*–pyrazole-3-carboxylic acid, Tp^* = hydrotris(3,5-dimethyl-pyrazolyl) borate, pzH^* = 3,5-dimethylpyrazole, HL_2 = 5-phenyl-1*H*-pyrazole-3-carboxylic acid) [27], $Tp^*VO(pzH^*)(CH_3COO)$, $Tp^*VO(pzH^*)(C_6H_5COO)$ and $Tp^*VO(pzH^*)(m\text{-}NO_2C_6H_4\text{-}COO)\cdot CH_3CN$ [28], which pertain to the mechanism of bromoperoxidation. However, hydrogen-bonding interaction for influence on this catalytic activity is rarely investigated.

In this manuscript, we report the syntheses, crystal structures and properties of three supramolecular complexes, $[VO(phen)(C_2O_4)(H_2O)]\cdot CH_3OH$ (**1**), $[(VO)_2(u_2C_2O_4)(C_2O_4)_2(H_2O)_2]\cdot L\cdot H_2O$ (**2**), and $[(4,4'\text{-bipy}H_2)_{0.5}]^+[VO_2(2,6\text{-dipic})]^-\cdot 2H_2O$ (**3**) (phen = 1, 10-phenanthroline, 4,4′-bipy = 4,4′–bipyridine, 2,6-dipic = 2,6-pyridinedicarboxylic, L = 1,4-bis((3,5-dimethyl-1*H*-pyrazol-1-yl)methyl)benzene). Bromination activity and influence of hydrogen-bonding interaction on bromination have also been investigated.

2. Experimental

2.1. *Materials and methods*

All chemicals were of analytical grade and used without purification. L was synthesized according to the literature method [29,30]. Elemental analyzes for C, H, and N were carried out on a Perkin Elmer 240C automatic analyzer. Infrared spectra were recorded on a JASCO FT/IR-480 spectrometer with pressed KBr pellets from 200 to 4000 cm^{-1}. UV–vis spectra were recorded on a JASCO V-570 spectrometer (200–2500 nm, as solid samples).

2.2. *Synthesis of the complexes*

2.2.1. $[VO(phen)(C_2O_4)(H_2O)]\cdot CH_3OH$ (1). $VO(acac)_2$ (0.27 g, 1.00 mmol), 1,10-phen (0.2 g, 1.00 mmol) and $H_2C_2O_4$ (0.13 g, 1.00 mmol), were dissolved in CH_3OH (10 mL)

and the mixture was stirred for 4 h at room temperature to give a green solution. Then, the solution was left at room temperature for a few days with green crystals obtained in *ca.* 37% yield based on V(IV). Anal. Calcd for $C_{15}H_{14}O_7N_2V$: C, 46.87; H, 3.65; N, 7.29. Found: C, 46.55; H, 3.46; N, 7.21%. IR (KBr, ν, cm^{-1}): 3408, 3060, 1715, 1693, 1649, 1386, 1517, 1424, 1230, 1142, 1105, 983, 451, 356. UV–vis (λ_{max}, nm): 262, 342, 440, 538, 722.

2.2.2. $[(VO)_2(u_2\text{-}C_2O_4)(C_2O_4)_2(H_2O)_2]\cdot L\cdot H_2O$ (2). **2** was synthesized by procedure similar to that for **1** but 1,10-phen was replaced by L in the reaction (0.29 g, 1.00 mmol) in C_2H_5OH (95%). Primrose blue crystals of **2** were obtained in *ca.* 33% yield (based on V(IV)). Anal. Calcd for $C_{24}H_{30}O_{18}N_4V_2$: C, 37.68; H, 3.92; N, 7.33. Found: C, 37.58; H, 3.88; N, 7.30%. IR (KBr, ν, cm^{-1}): 3426, 3148, 2976, 1715, 1672, 1630, 1399, 983, 479. UV–vis (λ_{max}, nm): 260, 342, 586, 728.

2.2.3. $[(4,4'\text{-bipyH}_2)_{0.5}]^+[VO_2(2,6\text{-dipic})]^-\cdot 2H_2O$ (3). $V_2(SO_4)_3$ (0.39 g, 1.00 mmol), 4,4′-bipy (0.16 g, 1.00 mmol), 2,6-dipic (0.17 g, 1.00 mmol) and H_2O (10 mL) were mixed and stirred for 2 h, the mixture sealed into a bomb and heated at 160 C for 4 days, cooled to room temperature and yellow crystals of **3** were obtained in *ca.* 45% yield (based on V (III)). Anal. Calcd for $C_{12}H_{12}O_8N_2V$: C, 39.65; H, 3.30; N, 7.71. Found: C, 39.56; H, 3.32; N, 7.83%. IR (KBr, ν, cm^{-1}): 3439, 3104, 3076, 1677, 1640, 1344, 1489, 1433, 1252, 1180, 1079, 958, 934, 470, 428, 360. UV–vis (λ_{max}, nm): 262, 304, 322.

2.3. *Single-crystal structural determinations*

The crystals of **1**, **2,** and **3** were mounted on glass fibers for X-ray measurement, respectively. Reflection data were collected at room temperature on a Bruker AXS SMART APEX II CCD diffractometer with graphite-monochromated Mo-Kα radiation ($\lambda = 0.71073$ Å) and a ω scan mode. All independent reflections ($I > 2\sigma(I)$) were used in the structural analyzes and semi-empirical absorption corrections were applied using SADABS [31]. The structures were solved by direct methods using SHELXL-97 [32]. All non-hydrogen atoms were refined anisotropically. Hydrogens were fixed at calculated positions geometrically and refined by using a riding model, except hydrogens of coordinated water in **1** and lattice waters and 4,4′-bipy in **3** were found in difference Fourier map. Crystallographic data and structure refinement details are given in table 1. Drawings were made with Diamond 3.2.

2.4. *Measurement of bromination activity in solution*

Bromination activity tests were carried out in mixed H_2O–DMF solution at 30 ± 0.5 C. Oxidovanadium complexes were dissolved by addition of 25 mL H_2O–DMF in volume ratio of 4 : 1. Solutions used for kinetic measurements were maintained at a constant concentration of H^+ (pH 5.8) by addition of the buffer solution of NaH_2PO_4–Na_2HPO_4 [14]. Reactions were initiated by addition of phenol red solution. Oxidovanadium complexes with five different concentrations were prepared in five cuvettes. The cuvettes were put in the constant temperature for 10 min, and spectral changes were recorded using a

Table 1. Crystallographic data and structure refinement for **1–3**.

Complexes	**1**	**2**	**3**
Formula	$C_{15}H_{12}N_2O_7V$	$C_{24}H_{30}N_4O_{18}V_2$	$C_{12}H_{12}N_2O_8V$
M (g mol^{-1})	383.21	764.40	363.18
Crystal system	Monoclinic	Triclinic	Monoclinic
Space group	*P*2(1)/c	*P*-1	*C*2/*c*
a (Å)	7.6720(15)	8.938(2)	25.904(3)
b (Å)	13.338(3)	9.607(3)	6.9066(8)
c (Å)	15.593(3)	9.641(2)	16.2790(19)
α (°)	90	85.289(3)	90
β (°)	97.499(3)	78.700(4)	106.164(2)
γ (°)	90	77.113(4)	90
V (Å^3)	1582.0(5)	790.7(3)	2797.4(6)
Z	4	1	8
D_{calc}	1.609	1.605	1.725
Crystal size (mm)	0.54 × 0.16 × 0.11	0.4 × 0.25 × 0.1	0.47 × 0.24 × 0.12
F(000)	780	392	1480
μ(Mo-Kα) / mm^{-1}	0.669	0.678	0.756
θ (°)	2.02–25.36	2.16–23.86	1.64–25.00
Reflections collected	7877	3589	4369
Independent reflections (I >2σ(*I*))	2882 (2251)	2402 (1585)	2339 (1794)
Parameters	234	217	220
$\Delta(\rho)$ (e Å^{-3})	0.658, −0.573	0.345, −0.323	0.631, −0.491
Goodness-of-fit	1.073	1.036	1.088
R^a	0.0497 (0.1331)[b]	0.0531 (0.1181)[b]	0.0431 (0.1118)[b]
wR_2[a]	0.0653 (0.1447)[b]	0.0905 (0.1350)[b]	0.0597 (0.1188)[b]

[a]$R = \sum ||F_o| - |F_c|| / \sum |F_o|$, $wR_2 = [\sum(w(|F_o|^2 - |F_c|^2)^2 / [\sum(w(|F_o|^2)^2]^{1/2}$; $[|F_o| > 4\alpha(|F_o|)]$.

721 UV–vis spectrophotometer every 5 min. The resulting data were collected and fitted using curve-fitting software in Microsoft Excel.

The rate of this reaction is described by the rate equation: $dc/dt = kc_1^x c_2^y c_3^z$, giving the equation "$\log(dc/dt) = \log k + x\log c_1 + y\log c_2 + z\log c_3$," corresponding to "$-\log(dc/dt) = -x\log c_1 - b(b = \log k + y\log c_2 + z\log c_3)$" where k is the reaction rate constant, c_1, c_2, c_3 are the concentrations of the complex, KBr and phenol red, respectively; x, y, and z are the corresponding reaction orders. According to Lambert-Beer's law, $A = \varepsilon \cdot d \cdot c$, where A is the measurable absorbance of the resultant, ε is molar absorption coefficient, which of bromophenol blue is measured as 14,500 M^{-1}cm^{-1} at 592 nm and d is light path length of sample cell (d = 1). When the measurable absorbance data were plotted versus reaction time, a line was obtained and the reaction rate of the complexes (dA/dt) was given by the slope of this line. By changing the concentration of oxovanadium complexes in the reaction system, a series of dA/dt data can be obtained. The reaction rate constant (k) can be obtained from a plot of $-\log(dc/dt)$ versus $-\log c_1$, fitted using the curve-fitting software in Microsoft Excel by generating a least squares fit to a general equation of the form "$y = mx - b$," in which "m" is the reaction order of the oxovanadium complexes in this reaction and "b" is the intercept of the line. In the experiment, considering that the reaction orders of KBr and phenol red (y and z) are 1 according to the literature; c_2 and c_3 are 0.4 and 10^{-4} mol/L, respectively. Based on the equation "$b = \log k + y\log c_2 + z\log c_3$," the reaction rate constant (k) can be obtained. Bromination of phenol red was monitored by measurement of the absorbance at 592 nm for reaction aliquots which were extracted at specific times and diluted into pH 5.8 phosphate buffer.

2.5. *Electrochemical determinations*

Electrochemical determinations were performed by cyclic voltammetry in DMF in the potential range from 1000 to −1200 mV using a MCP-1 Potentiostat/Galvanostat and a home-built computer-controlled instrument based on the ZF-10B data acquisition board (National Instruments). A three-electrode cell was used, in which a platinum wire electrode was the working electrode, a saturated Ag/AgCl electrode was the reference electrode, and another platinum wire was the auxiliary electrode. The electrodes were rinsed with deionized water between each grade. The concentration of the complex is 1.0×10^{-4} mol L^{-1}. Cyclic voltammetric current-potential (i–E) curves were used to assess heterogeneous electron transfer, where i is the Faradaic current at the formal reduction potential (E).

3. Results and discussion

3.1. *Synthesis*

Both **1** and **2** were synthesized by reaction of $VO(acac)_2$ as starting material at room temperature with methanol and ethanol. To obtain single crystals suitable for X-ray diffraction, we have screened solvents, showing that methanol was best for **1**, while ethanol was suitable for **2**. Although the molecular structure of **3** was been reported, the synthetic method and starting material used in this work were different from those in the literature [33]. Starting materials of V(III) used in the synthesis of **3**, while oxidation state of vanadium of the corresponding complex is +5, were further confirmed by Bond-Valence Theory [34,35]. It is easy to oxidize V(III) by oxygen from the air [36]. **1**, **2,** and **3** are all quite stable at room temperature; **1** and **2** are easily soluble in DMF and CH_2Cl_2, slightly in methanol and water, and insoluble in hexane and ether, while **3** is slightly soluble in DMF and insoluble in other solvents.

3.2. *Spectra properties*

3.2.1. IR spectra. For **1–3** (Supplementary material), spectra have bands at 3408–3439 cm^{-1} assigned to O-H stretches and bands at 3060–3148 cm^{-1} assigned to =C–H stretches. The band at 2976 cm^{-1} for **2** is assigned to $–CH_3$ stretch. The asymmetric $\nu_{as(COO–)}$ and symmetric $\nu_s(COO^-)$ stretches of deprotonated carboxylates are 1640–1693 and

Table 2. Characteristic IR bands (cm^{-1}) for **1**–**3**.

Complex	**1**	**2**	**3**
$\nu_{(O–H)}$	3408	3426	3439
$\nu_{(=C–H)}$	3060	3148	3104, 3076
$\nu_{as(–CH3)}$	–	2976	–
$\nu_{(C=N)}$	1715	1715	1677
$\nu_{as}(COO^-)$	1693, 1649	1672, 1630	1640
$\nu_s(COO^-)$	1386	1399	1344
Pyridine/pyrazolyl	1517, 1424, 1230, 1142, 1105	–	1489, 1433 , 1252, 1180, 1079
$\nu_{(V=O)}$	983	983	958, 934
$\nu_{(V–O)}$	451	479	470, 428
$\nu_{(V–N)}$	356	–	360

1344–1399 cm^{-1}, respectively. V=O bands were 934–983 cm^{-1}, V–O at 428–480 cm^{-1}, and V–N at 350–360 cm^{-1} [37]. Detailed assignments of IR spectra for **1–3** are shown in table 2.

3.2.2. UV–vis absorption spectra. UV–vis absorption spectra of **1**, **2,** and **3** (Supplementary material) are recorded as solid samples and their characteristic UV–vis bands are listed in table 3. The high-frequency absorptions at 260–262 nm are assigned to π–π^* transitions of the aromatic-like chromophore from 1,10-phenanthroline, L, 2,6-dipic acid and 4,4′-bipy [38]. For vanadyl(IV) complexes, it is generally considered that transitions occur from d_{xy} to (d_{xz}, d_{yz}) (ν_1), $d_x^2 - d_y^2$ (ν_2) and d_z^2 (ν_3) orbitals with increasing energies. The absorptions at 304–440 nm are attributed to LMCT (ligand to metal charge transfer) transition. Complexes **1** and **2** exhibit two sets of absorptions with maximum wavelength at 722–728 and 538–586 nm, which can be assigned to (ν_1) and (ν_2) bands of oxovanadium (IV) [39].

3.3. *Structural description of 1–3*

The molecular structures of **1** and **2** are depicted in figures 1 and 3, respectively. The principal bond distances and angles for **1–3** are summarized in table 4. Deviations of the coordinated atoms out of the equatorial plane for **1–3** are listed in Supplementary Material. There are abundant inter-and intra-molecular hydrogen bonds in the three complexes. Relevant H-bond parameters of **1**, **2,** and **3** are listed in table 5.

Table 3. Characteristic UV-vis bands (nm) for **1**–**3**.

Complex	π–π^* transition	LMCT	d–d transition
1	262	342, 440	538, 722
2	260	342	586, 728
3	262	304, 322	–

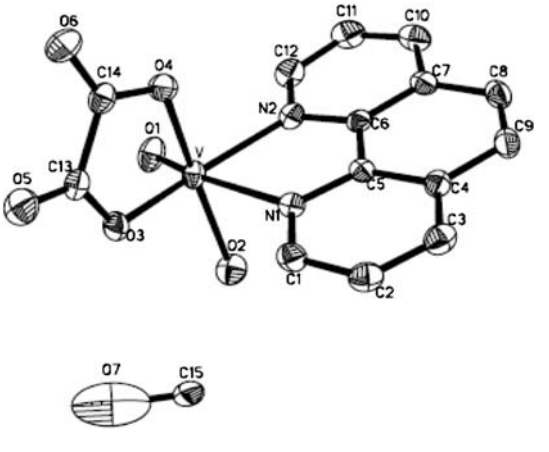

Figure 1. The molecular structure of **1** (all hydrogens are omitted for clarity).

Table 4. Selected bond lengths (Å) and angles (°) for **1**–**3**.

*Complex **1***			
V–O1	1.588(3)	O2–V–N2	96.65(13)
V–O2	2.048(3)	O1–V–N1	165.14(12)
V–O3	1.979(2)	O3–V–N1	86.39(10)
V–O4	2.001(2)	O4–V–N1	87.62(10)
V–N1	2.322(3)	O2–V–N1	78.61(11)
V–N2	2.123(3)	N2–V–N1	73.81(10)
O1–V–O3	107.43(13)	O4–V–O2	164.21(13)
O1–V–O4	99.73(13)	O1–V–N2	93.59(13)
O3–V–O4	80.86(10)	O3–V–N2	157.07(11)
O1–V–O2	95.45(14)	O4–V–N2	86.76(10)
O3–V–O2	90.51(13)		
*Complex **2***			
V1–O1	1.571(3)	O4–V1–O7	92.04(14)
V1–O2	2.027(3)	O1–V1–O2	99.80(17)
V1–O3	1.975(3)	O3–V1–O2	89.61(14)
V1–O4	2.000(3)	O4–V1–O2	160.18(15)
V1–O7	2.020(3)	O7–V1–O2	89.45(13)
V1–O8	2.284(3)	O1–V1–O8	171.86(16)
O1–V1–O3	104.87(16)	O3–V1–O8	82.62(13)
O1–V1–O4	99.62(17)	O4–V1–O8	78.06(13)
O3–V1–O4	81.58(14)	O7–V1–O8	75.15(12)
O1–V1–O7	97.25(16)	O2–V1–O8	83.24(13)
O3–V1–O7	157.70(13)		
*Complex **3***			
V–O1	1.602(2)	O2–V–O4	97.41(11)
V–O2	1.614(2)	O1–V–O3	100.29(11)
V–O3	1.993(2)	O2–V–O3	98.78(10)
V–O4	1.990(2)	O4–V–O3	148.46(9)
V–N1	2.089(2)	O1–V–N1	117.47(11)
O1–V–O2	109.37(13)	O2–V–N1	133.14(11)
O1–V–O4	99.59(11)	O4–V–N1	74.44(9)
O3–V–N1	74.72(9)		

For **1**, vanadium is coordinated by a terminal oxygen (O6), one oxygen (O5) from coordinated water, two oxygens (O1, O2) from oxalate, and two nitrogens (N1, N2) from 1,10-phenanthroline to form a distorted octahedral vanadium with O2, O3, O4, and N2 in the equatorial plane, O1 and N1 in axial positions. The deviations of O2, O3, O4, and N2 from the least-squares plane are 0.0494, −0.0597, 0.0603, and −0.0500 Å, respectively, showing that these atoms are almost in one plane. The V, O1, and N1 from axial positions lay 0.3121, 1.8887, and −1.9865 Å out of the equatorial plane, with V toward the *oxo* O1, *trans* to N1, a consequence of the strong *trans* influence of the terminal *oxo* group. The O1−V−N1 angle is 165.14(12)°. By comparison, the order of the bond lengths of V–O is $V–O2_{water} > V–O4_{carboxyl} > V–O3_{carboxyl}$, which indicates that the coordination ability of oxalate is stronger than that of coordinated water.

There are two types of hydrogen bonds in **1** as shown in figure 2, O–H···O (2.9151–2.9869 Å) and C–H···O (3.1861 Å). Hydrogen bonds of O–H···O are between coordinated water (O2) and carboxyl oxygen ($O5^{\#1}$ and $O6^{\#1}$, #1: 1 + x, y, z) of oxalate; hydrogen bond of C–H···O is between 1,10-phenanthroline (C2) and terminal oxygen (O1). By C2–H2A···O1 hydrogen bond, molecules are linked to form a 1-D chain along the *b*-axis. Adjacent chains are connected through O2–H14A···$O5^{\#1}$ and O2–H14A···$O6^{\#1}$ hydrogen bonds to form a 2-D supramolecular structure.

Structural analysis for **2** shows that there are two vanadiums, three oxalates, two coordinated waters, and one free L in the asymmetric unit. Complex **2** consists of L and

Table 5. Hydrogen bonds (Å) of **1**–**3**.

D–H···A	d(D–H) (Å)	d(H···A) (Å)	d(D···A) (Å)	∠D–H···A (°)
Complex ***1***				
O2–H14A···O5$^{\#1}$	0.7862	2.3840	2.9869	134.34
O2–H14A···O6$^{\#1}$	0.7862	2.2093	2.9151	149.67
C2–H2A···O1	0.9300	2.5450	3.1861	126.40
Complex ***2***				
O1w–H1wB···O5	0.9000	2.3332	3.1756	155.77
O1w–H1wB···O6	0.9000	2.2774	2.9084	126.92
O2–H23B···O1w	0.7500	1.9230	2.6412	160.32
O2–H23A···O3$^{\#2}$	0.9000	1.8303	2.7249	172.32
C2–H2A···O1$^{\#1}$	0.9600	2.5501	3.3295	138.39
C3–H3A···O7$^{\#3}$	0.9300	2.4363	3.3591	171.64
C9–H9···O5	0.9300	2.5984	3.4974	162.74
Complex ***3***				
N2$^{\#4}$–H2$^{\#4}$···O2w$^{\#4}$	0.9462	1.7312	2.6649	168.44
O1w$^{\#2}$–H1wB$^{\#3}$···O6$^{\#3}$	0.8500	2.3746	2.9610	126.59
O2w$^{\#4}$–H2wB$^{\#4}$···O5$^{\#2}$	0.8633	2.1566	3.0077	168.58
O2w$^{\#4}$–H2wA$^{\#4}$···O1w$^{\#1}$	0.7349	2.3500	2.9943	147.18
O2w–H2wA···O5	0.7349	2.5100	2.9504	120.35
C12$^{\#4}$–H1$^{\#4}$···O4$^{\#2}$	0.9300	2.3565	3.2674	166.30
C3–H3···O1	0.9300	2.5087	3.3313	147.58
C9$^{\#4}$–H7$^{\#4}$···O1w$^{\#4}$	0.9300	2.4583	3.3828	172.68

Symmetry transformation used to generate equivalent atoms: **1** (#1 : $1+x$, y, z); **2** (#1: $-x$, $-y+1$, $-z+1$; #2: $-x+1$, $-y$, $-z$; #3: $-x$, $-y$, $1-z$); **3** (#1: $-x$, y, $0.5-z$; #2: x, $-y$, $0.5+z$; #3: x, $y-1$, z; #4: $-x$, $-y$, $1-z$).

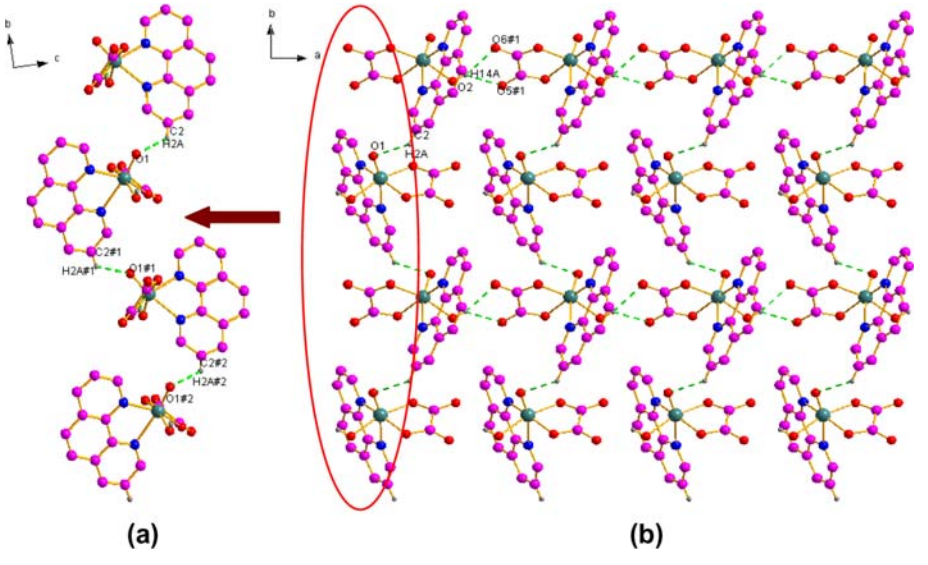

Figure 2. (a) Fragment of 1D chain network of hydrogen bonding along the *b*-axis; (b) A view of two-dimensional hydrogen bonding network in **1**. (All hydrogens except for hydrogen bonds are omitted for clarity).

binuclear V-oxalate complex moiety with hydrogen-bonding interaction. The binuclear anion is centrosymmetric with the center of inversion lying on the C−C bond of the bridging oxalate [33]. The same coordination environment of the two vanadiums is observed and we take one as an example. The oxidation state of vanadium is +4,

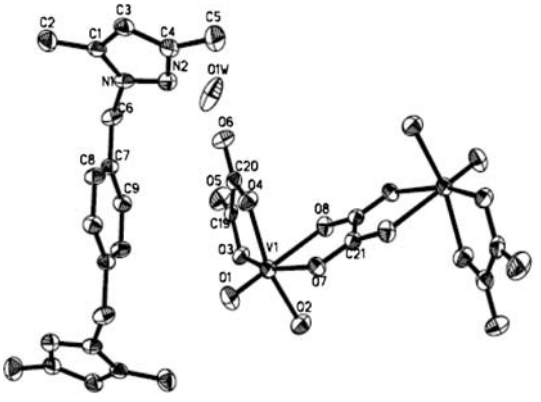

Figure 3. The molecular structure of **2** (all hydrogens are omitted for clarity).

confirmed by Bond-Valence Theory. Vanadium is coordinated by a terminal oxygen (O1), one oxygen (O2) from coordinated water, and four oxygens (O3, O4, O7, O8) from oxalate to form an axial *trans* octahedron with O2, O3, O4, and O7 in the equatorial plane and O1 and O8 in axial positions. The deviations of O2, O3, O4, and O7 from the least-squares plane are −0.0233, 0.0255, −0.0249, and 0.0226 Å, respectively, with V1, O1, and O8 from axial positions lying −0.3594, −1.9281, and 1.9167 Å out of the equatorial plane, indicating that vanadium is displaced toward the *oxo* oxygen O1, forming the angle of O1–V1–O8 of 171.86(16)°. The bond length order of V–O (V–O2, V–O3 and V–O4) is $V–O2_{water} > V–O4_{carboxyl} > V–O3_{carboxyl}$, similar to those in **1**. The order of the bond lengths of $V–O_{carb}$ from oxalate is V–O8 > V–O7 > V–O4 > V–O3, because O7 and O8 are bridging, and O8 is *trans* to terminal *oxo*.

There are two types of hydrogen bonds, O–H···O (2.6412–3.1756 Å) and C–H···O (3.3295–3.3591 Å) in **2**, as illustrated in figure 4(a). O–H···O hydrogen bonds are between coordinated water (O2) and carboxyl oxygen ($O3^{\#2}$, #2: −x + 1, −y, −z) of coordinated oxalate, coordinated water (O2) and lattice water (O1w), lattice water (O1w), and carboxyl (O5 and O6), respectively; C–H···O hydrogen bonds come from C2 in methyl of the uncoordinated L and terminal oxygen ($O1^{\#1}$, #1: −x, −y + 1, −z + 1), C3 in pyrazolyl of L and oxygen ($O7^{\#3}$, #3: -x, -y, 1-z) in bridging positions, respectively. The coordinating vanadium via $O2–H23A\cdots O3^{\#2}$ along the *b*-axis becomes a 1-D chain, and then, adjacent chains are connected to organic ligands (L) via $C2–H2A\cdots O1^{\#1}$ and $C3–H3A\cdots O7^{\#3}$ to form a 2-D sheet structure. Numerous O–H···O hydrogen-bonding interactions involving coordinated water of one layer and coordinated oxalate of the adjacent layer via lattice water are established (O1w–H1wB···O5, O1w–H1wB···O6 and O2–H23B···O1w), as shown in figure 4(b). Consequently, these hydrogen bond interactions combine to form a 3-D hydrogen-bonding network.

For **3**, the structure can be evaluated by the Addison distortion index τ [40]: $\tau = |\beta - \alpha|/60°$, β is the greater of the basal angles of the axial ligand. In a five-coordinate system, values for τ are 1.0 for trigonal bipyramidal and 0.0 for square pyramidal [41]. The value of τ for **3** is 0.65, indicating that the coordination environment of V(V) is close to distorted trigonal bipyramidal. Comparison of related bond lengths of **3** found that (i) the V–O1 bond length (1.606(2) Å) is shorter than those in $C(NH_2)_3[VO_2(dipic)]\cdot 2H_2O$, $NH_4[VO_2(dipic)]$ [42], $[CH_3NHC(NH_2)_2]_2[V_2O_4(dipic)_2]$ [43] and $K[VO_2(dipic\text{-}OH)]\cdot H_2O$

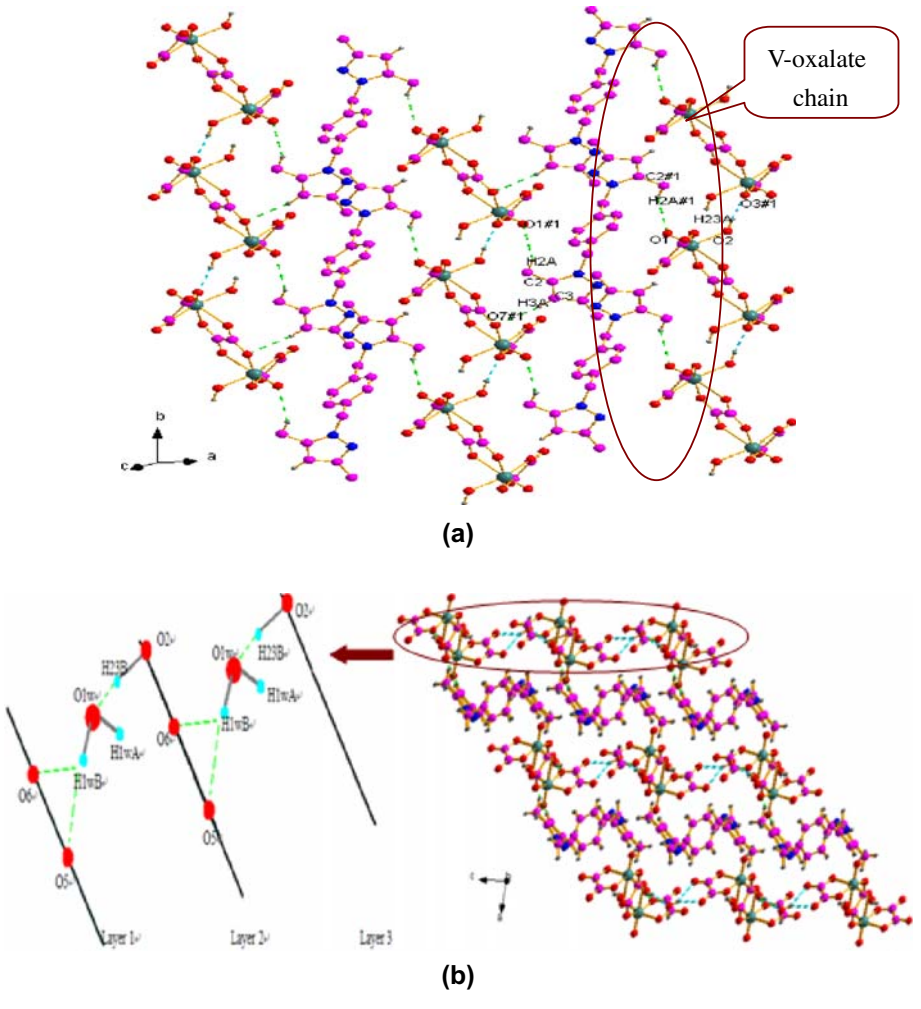

Figure 4. (a) A view of two-dimensional hydrogen bonding network in **2**; (b) A view of 3D hydrogen bond network in **2**. (All hydrogens except for hydrogen bonds are omitted for clarity).

Table 6. Comparison of the bond lengths (Å) in related complexes.

Complex	V=O	V-O_{carb1}	V-O_{carb2}	V-N	Ref.
$C(NH_2)_3[VO_2(dipic)]\cdot H_2O$	1.614(7)	1.983(2)	1.988(2)	2.086(2)	[42]
$NH_4[VO_2(dipic)]$	1.624(2)	1.974(2)	1.978(2)	2.091(2)	[42]
$[CH_3NHC(NH_2)_2]_2[V_2O_4(dipic)_2]$	1.606(1)	1.995(1)	1.984(1)	2.097(2)	[43]
(4,4'-bipy)$[VO_2(dipic)]_2\cdot 2H_2O$	1.602(2)	1.993(2)	1.990(2)	2.089(2)	This work
$NH_4[VO(O_2)(H_2O)(dipic)]\cdot xH_2O$ ($x = 1.3$)	1.579(2)	2.053(2)	2.064(2)	2.088(2)	[45]
$K[VO(O_2)(DL\text{-}cmhist)]\cdot H_2O$	1.598(1)	2.144(1)	2.045(1)	2.169(2)	[46]
$K[VO_2(dipic\text{-}OH)]\cdot H_2O$	1.616(5)	1.990(5)	2.033(5)	2.089(6)	[44]
$VO(H_2O)_2(dipic)\cdot 2H_2O$	1.594(3)	2.026(3)	2.051(4)	2.163(4)	[47]

[44] and slightly longer than $NH_4[VO(O_2)(H_2O)(dipic)]\cdot xH_2O$ ($x \approx 1.3$) [45], $K[VO(O_2)(DL\text{-}cmhist)]\cdot H_2O$ (H_2cmhist = DL-N-carboxymethylhistidine) [46] and $VO(H_2O)_2(dipic)\cdot 2H_2O$ [47]. (ii) The V–N bond length is similar to those corresponding to the complexes

Table 7. Comparison of the angles (°) in related complexes.

Complex	N–V=O	O=V–O_{carb}	O=V–O_{carb2}	N–V–O_{carb}	Ref.
$C(NH_2)_3[VO_2(dipic)]\cdot H_2O$	124.6(4), 125.4(4)	98.8(3), 98.3(3)	99.9(3), 97.8(3)	74.73(6), 74.82(6)	[42]
$NH_4[VO_2(dipic)]$	124.86(8), 124.86(8)	98.40(8), 101.38(9)	97.66(8), 98.49(9)	74.64(7), 4.72(7)	[42]
$[CH_3NHC(NH_2)_2]_2[V_2O_4(dipic)_2]$	100.08(7), 154.56(6)	96.11(6), 97.54(6)	101.38(6), 148.46(5)	74.80(6), 74.90(6)	[43]
(4,4′-bipy)$[VO_2(dipic)]_2\cdot 2H_2O$	117.47(11)	99.59(11)	100.29(11)	74.44(9)–74.72(9)	This work
$NH_4[VO(O_2)(H_2O)(dipic)]\cdot xH_2O$ ($x = 1.3$)	92.2 (1)	96.2 (1)	94.9 (1)	74.5(1)–74.3(1)	[45]
$K[VO(O_2)(DL\text{-}cmhist)]\cdot H_2O$	92.00(7)	167.47(7)	95.73(6)	75.68(6)–77.60(6)	[46]
$K[VO_2(dipic\text{-}OH)]\cdot H_2O$	123.1(3)–127.4(3)	98.0(2)–99.4(3)	98.8(3)–100.4(3)	73.3(2)–74.7(2)	[44]
$VO(H_2O)_2(dipic)\cdot 2H_2O$	178.07(11)	106.40(17)	87.27(16)	73.39(15)–73.75(15)	[47]

above, as shown in table 6. (iii) The N–V=O and O=V–O_{carb} angles are 99.59(11)° and 100.29(11)° in **3**, respectively. Both angles are larger than those in $C(NH_2)_3[VO_2(dipic)]\cdot H_2O$, $NH_4[VO_2(dipic)]$, $NH_4[VO(O_2)(H_2O)(dipic)]\cdot xH_2O$ ($x \approx 1.3$) and $K[VO_2(dipic\text{-}OH)]\cdot H_2O$, while the N–V–$O_{carb}$ angles are close to those found in other vanadium complexes (table 7).

In the molecular packing of **3**, there are three types of hydrogen bonds, N–H···O (2.6649 Å), O–H···O (2.9504–3.0077 Å) and C–H···O (3.2674–3.3828 Å). The N–H···O hydrogen bond comes from 4,4′-bipy ($N2^{\#4}$, #4: -x, -y, 1-z) and lattice water ($O2w^{\#4}$). The

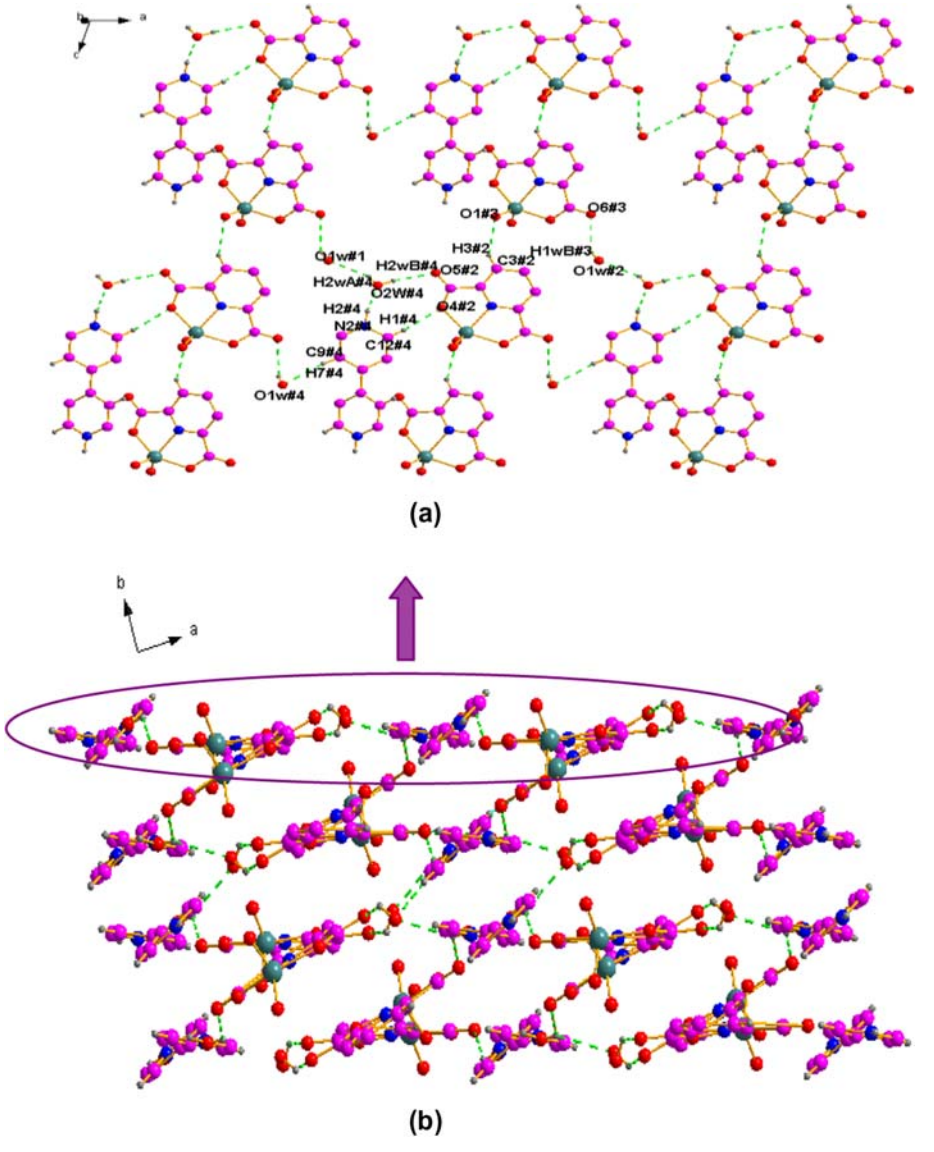

Figure 5. (a) A view of two-dimensional hydrogen bonding network in **3**; (b) A view of 3D hydrogen bond network in **3**. (All hydrogens except for hydrogen bonds are omitted for clarity).

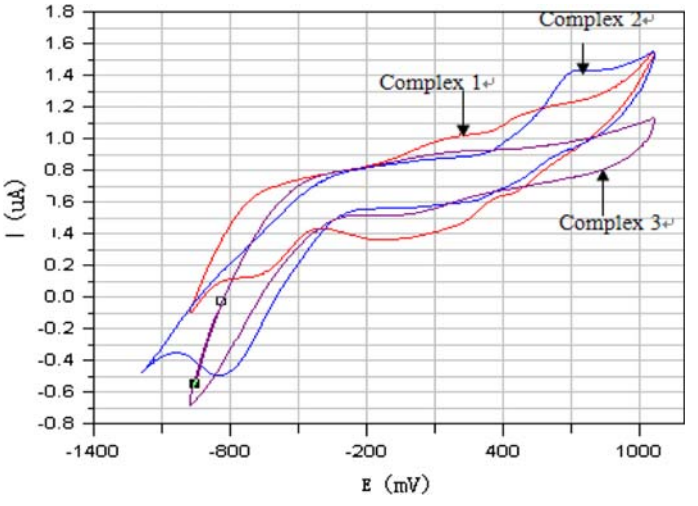

Figure 6. Cyclic voltammograms for **1**–**3** in DMF; scan rate = 80 mV/s

O–H···O hydrogen bonds come from lattice water (O1w$^{\#1}$, #1: −x, y, 0.5−z and O2w$^{\#4}$), the lattice water (O2w$^{\#4}$ and O1w$^{\#2}$, #2: x, −y, 0.5 + z) and carboxyl oxygen (O5$^{\#2}$ and O6$^{\#3}$, #3: x, y−1, z) of 2,6-dipic; C–H···O hydrogen bonds are from C12$^{\#4}$ of 4,4′-bipy and carboxyl oxygen (O4$^{\#2}$) of 2,6-dipic, C3 in pyridyl ring of 2,6-dipic and terminal oxygen (O1), C9$^{\#4}$ of 4,4-bipy and lattice water (O1w$^{\#4}$), respectively. Independent molecules are linked to form a 2-D sheet structure with C–H···O and O–H···O hydrogen bonds (C12$^{\#4}$–H1$^{\#4}$···O4$^{\#2}$, C3–H3···O1, C9$^{\#4}$–H7$^{\#4}$···O1w$^{\#4}$, O1w$^{\#2}$–H1wB$^{\#3}$···O6$^{\#3}$, O2w$^{\#4}$–H2wB$^{\#4}$···O5$^{\#2}$, O2w$^{\#4}$–H2wA$^{\#4}$···O1w$^{\#1}$, N2$^{\#4}$–H2$^{\#4}$···O2w$^{\#4}$). Adjacent sheets are connected through hydrogen bonds O2w–H2wA···O5, C9$^{\#2}$–H7$^{\#2}$···O1w$^{\#2}$ and C12$^{\#2}$–H1$^{\#2}$···O4$^{\#4}$ to form a 3-D crossed supramolecular structure, as illustrated in figure 5.

3.4. *Analysis of redox behavior*

The redox behaviors of **1**–**3** were studied using cyclic voltammetry. As shown in figure 6, the cyclic voltammogram of **2** exhibits one redox couple with the oxidation wave at 745 mV and the corresponding reduction peak at −849 mV, which could be assigned to the process V(IV/V). The reduction peak of **1** is observed at −702 mV. However, it is hard to observe the oxidation wave due to electron donating 1,10-phen. The redox couple was not observed in **3**, due to the highest oxidation state of vanadium(V) already established. The peak shape of **2** is stable, explaining that reduction product could be oxidized sequentially on the electrode, so it was a reversible process; oxidation and reduction of **1** and **3** were irreversible.

3.5. *Functional mimics of the vanadium haloperoxidases*

3.5.1. Mimicking bromination reaction of the complexes. Oxidovanadium complexes are able to mimic the reaction in which vanadium haloperoxidases catalyze the bromination of organic substrates in the presence of H_2O_2. For example, the bromination

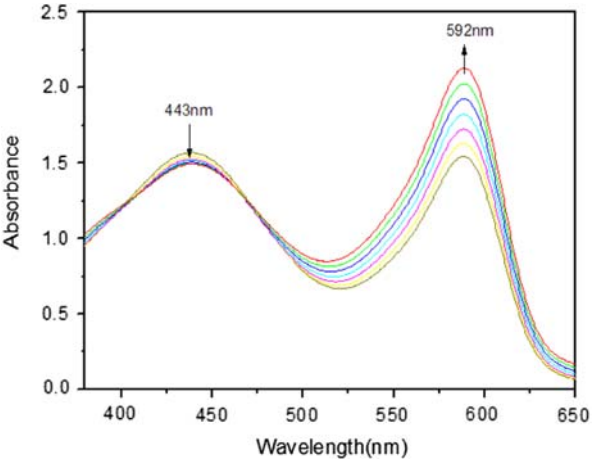

Figure 7. Oxidative bromination of phenol red catalyzed by **2**. Spectral changes at 10 min intervals. The reaction mixture contained phosphate buffer (pH 5.8), KBr (0.4 mol L^{-1}), phenol red (10^{-4} mol L^{-1}) and **2** (0.1 μmol L^{-1}).

of trimethoxybenzene [48], benzene, salicylaldehyde and phenol catalyzed by the VO_2^+ moiety [49] and the bromination of phenol red by $[VO(O2)H_2O]^+$ and related species [50] have been reported. Herein, the bromination reaction activities of **1**, **2**, and **3** using phenol red as substrate is shown by conversion of phenol red to bromophenol blue. The reaction is rapid and stoichiometric, producing halogenated product by reaction of oxidized halogen species with the organic substrate.

Addition of solution of **2** to bromide in phosphate buffer with phenol red as a trap for oxidized bromine resulted in color change of the solution from yellow to blue. As shown in figure 7, decrease in absorbance of the peak at 443 nm due to the loss of phenol red and increase in the absorbance of the peak at 592 nm characteristic of the bromophenol blue product show that **2** performs significant catalytic activities. The results of the mimic catalytic activities for **1** and **3** are similar to that of **2**.

3.5.2. Kinetic studies of bromination. A series of dA/dt data for **2** was obtained (figure 8) by changing the concentration of the oxovanadium complex. (The absorbance dependence of time for **1** and **3** are shown in Supplementary material).

The plot of $-\log(dc/dt)$ versus $-\log c$ for **2** gave a straight line with a slope of 1.0025 and $b = -1.3$, as shown in figure 9. The former confirms the first-order dependence on vanadium. Based on "$b = \log k + y\log c_2 + z\log c_3$," the reaction rate constant, k, is determined by the concentrations of KBr and phenol red (c_2 and c_3), the reaction orders of KBr and phenol red (y and z) and b. Considering the reaction orders of KBr and phenol red (y and z) are 1 according to the literature [51,52], c_2 and c_3 are 0.4 and 10^{-4} mol L^{-1}, respectively, so the reaction rate constant (k) for **2** can be calculated as 1.253×10^4 $(mol/L)^{-2}$ s^{-1}. (–log(dc/dt) dependences of –log$c$ for **1** and **3** are shown in Supplementary Material).

Kinetic data for **1**, **2,** and **3** in DMF–H_2O at 30 ± 0.5 °C are shown in table 8. The reaction orders of the oxidovanadium complex in bromination reaction are all close to 1, confirming the first-order dependence on vanadium; the order of the reaction rate constant is **1** > **2** > **3**.

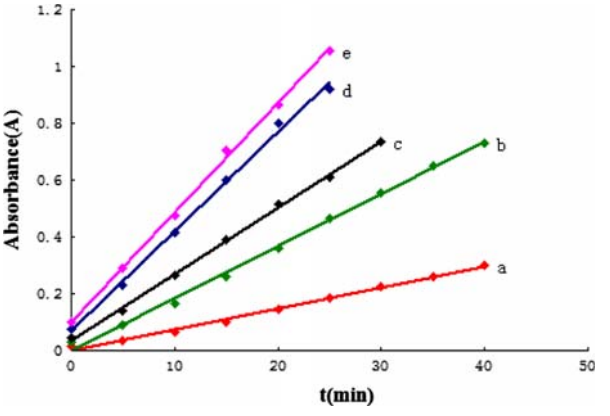

Figure 8. The measurable absorbance dependence of time for **2**. Conditions used: pH = 5.8, c(KBr) = 0.4 mol/L, c(H_2O_2) = 1 mmol/L, c(phenol red) = 10^{-4} mol/L. c(complex **2**/mmol/L) = a: 1.13×10^{-2}; b: 2.25×10^{-2}; c: 3.38×10^{-2}; d: 4.50×10^{-2}; e: 5.63×10^{-2}.

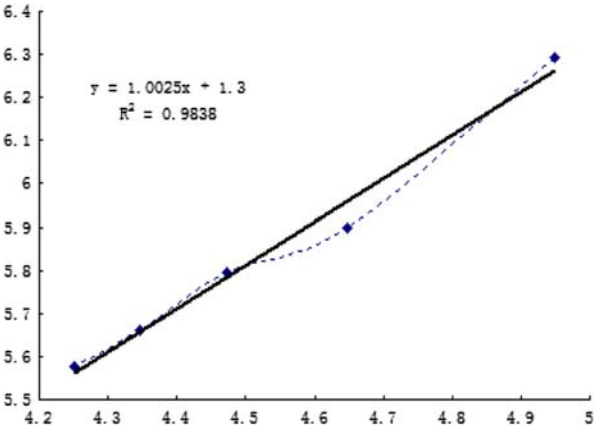

Figure 9. –log(dc/dt) dependence of –logc for **2** in DMF–H_2O at 30 ± 0.5 °C (c is the concentration of **2**. Conditions used: c(phosphate buffer) = 50 mmol/L, pH = 5.8, c(KBr) = 0.4 mol/L, c(phenol red) = 10^{-4} mol/L.

Table 8. Kinetic data for the complexes in DMF–H_2O at 30 ± 0.5°C*.

Complex	x	b	k (mol/L)$^{-2}$ s^{-1}	Ref.
1	1.1256	−1.0663	2.146×10^4	This work
2	1.0025	−1.3	1.253×10^4	This work
3	1.0255	−1.4756	8.36×10^3	This work
4	1.0076	−2.3524	1.116×10^3	[54]
5	0.9986	−2.7355	0.462×10^3	[55]
6	1.02	−2.7758	0.421×10^3	[55]
7	1.1153	−1.1672	2.347×10^3	[56]
8	0.9921	−1.4858	1.003×10^3	[56]

4: VO(HB(3,5-Me_2pz)$_3$)(3,5-Me_2pz)(HOOCCH$_2$CH$_2$COO); **5**: [VO(sal-ala)(2,2'bipy)]·H_2O; **6**: [VO(sal-ala)(1,10-phen)]·0.5H_2O; **7**: [VO(C_2O_4)(2,2′bipy)(H_2O)]·C_2H_5OH; **8**: [VO(C_2O_4)(phen)]·H_2O (H_2sal-ala: Schiff base derived from salicylaldehyde and DL-α-alanine).

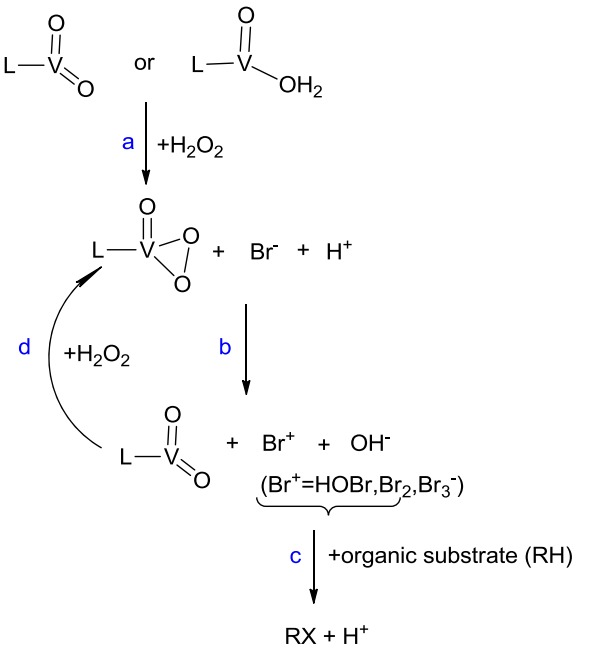

Scheme 1. The catalytic bromination reaction mechanism.

The catalytic bromination reaction mechanism is shown in scheme 1, in which in step a vanadium complexes are easily oxidized to $[VO(O_2)L]$ with H_2O_2 as a oxidation reagent; in step b Br^- is oxidized rapidly by $[VO(O_2)L]$, forming Br^+ and $[VO_2L]$. Catalytic reaction rate would be mainly based on the stability of the formed $[VO(O_2)L]$ (from step a to b) [50]. Comparison of kinetic data for the complexes reported previously is listed in table 8. The order of the reaction rate constant is **1** > **2** > **3** > **7** > **4** > **8** > **5** > **6**. The complexes **4–8** were synthesized according to references [53,18,54]. The complexes **1**, **2**, **3**, **7,** and **8** contain oxalate, and **1–3** and **7** have higher catalytic activities on bromination. Complex **8** is relatively lower, possibly due to its molecular structure being stable and more difficult to form $[VO(O_2)L]$. Complexes **5** and **6** have the lowest activities, probably because of the effect of the Schiff base ligands.

Catalytic activities of **1–3** are higher than the others, and the amounts and kinds of the hydrogen bonding should be also considered. We presume that lower dimension hydrogen-bonding network could favor formation of the intermediate of $[VO(O_2)L]$, further enhancing catalytic bromination activity.

4. Conclusion

To explore model oxovanadium complexes for the active centre of VHPO, we synthesized three supramolecular oxovanadium complexes and tested the bromination reaction activity with phenol red as organic substrate in the presence of H_2O_2, KBr, and phosphate buffer. Structural analysis shows that vanadium of **1** and **2** are six coordinate with distorted octahedral geometry, while **3** is five coordinate with distorted trigonal bipyramidal geometry.

There are abundant inter-molecular hydrogen bonds to form 1-D, 2-D and 3-D supramolecular structures. These intermolecular hydrogen bond networks may influence catalytic bromination activity.

Supplementary material

Tables of atomic coordinates, isotropic thermal parameters, and complete bond distances and angles have been deposited with the Cambridge Crystallographic Data Center. Copies of this information may be obtained free of charge by quoting the publication citation and deposition numbers CCDC: 873784 for **1**, 873785 for **2**, from the Director, CCDC, 12 Union Road, Cambridge CB2 1EZ, UK (Fax: +44 1223 336033; Email: deposit@ccdc.cam.ac.uk or http://www.ccdc.cam.ac.uk).

Acknowledgements

This study was supported by the grants of the National Natural Science Foundation of China (No. 21071071) and Dr start Foundation of Liaoning province in China (No. 20111067) for financial assistance.

References

[1] W. Plass. *Coord. Chem. Rev.*, **255**, 2378 (2011).
[2] E. Lodyga-Chruscinska, G. Micera, E. Garribba. *Inorg. Chem.*, **50**, 883 (2011).
[3] C. Wikete, P. Wu, G. Zampella, L.D. Gioia, G. Licini, D. Rehder. *Inorg. Chem.*, **46**, 196 (2007).
[4] D. Wischang, O. Brücher, J. Hartung. *Coord. Chem. Rev.*, **255**, 2204 (2011).
[5] I. Lippold, K. Vlay, H. Gorls, W. Plass. *J. Inorg. Biochem.*, **103**, 480 (2009).
[6] T.F.S. Silva, K.V. Luzyanin, M.V. Kirillova, M.F.G. da Silva, L.M.D.R.S. Martins, A.J.L. Pombeiro. *Adv. Synth. Catal.*, **352**, 171 (2010).
[7] D. Maity, J. Marek, W.S. Sheldrick, H. Mayer-Figge, M. Ali. *J. Mol. Catal.*, **270**, 153 (2007).
[8] M.R. Maurya, S. Agarwal, C. Bader, D. Rehder. *Eur. J. Inorg. Chem.*, 147, (2005).
[9] M. Ahmed, P. Schwendt, J. Marek, M. Sivak. *Polyhedron*, **23**, 655 (2004).
[10] M. Andersson, A. Willetts, S. Allenmark. *J. Org. Chem.*, **62**, 8455 (1997).
[11] H.B. ten Brink, H.E. Schoemaker, R. Wever. *Eur. J. Biochem.*, **268**, 132 (2001).
[12] V. Trevisan, M. Signoretto, S. Colonna, V. Pironti, G. Strukul. *Angew. Chem. Int. Ed.*, **43**, 4097 (2004).
[13] J. Gätjens, B. Meier, T. Kiss, E.M. Nagy, P. Buglyó, H. Sakurai, K. Kawabe, D. Rehder. *Chem. Eur. J.*, **9**, 4924 (2003).
[14] E. Verhaeghe, D. Buisson, E. Zekri, C. Leblanc, P. Potin, Y. Ambroise. *Anal. Biochem.*, **379**, 60 (2008).
[15] M. Časný, D. Rehder. *Dalton Trans.*, 839 (2004).
[16] D. Rehder. *Bioinorganic Vanadium Chemistry*, John Wiley & Sons, Hamburg (2008).
[17] S. Sarmah, D. Kalita, P. Hazarika, R. Borah, N.S. Islam. *Polyhedron*, **23**, 1097 (2004).
[18] Y.Z. Cao, H.Y. Zhao, F.Y. Bai, Y.H. Xing, D.M. Wei, S.Y. Niu, Z. Shi. *Inorg. Chim. Acta*, **368**, 223 (2011).
[19] T. Kojima, M.R. Antonio, T. Ozeki. *J. Am. Chem. Soc.*, **133**, 7248 (2011).
[20] M.I. Khan, Y.D. Chang, Q. Chen, J. Salta, Y.S. Lee, C.J. O'Connor, J. Zubieta. *Inorg. Chem.*, **33**, 6340 (1994).
[21] J. Salta, C.J. O'Connor, S. Li, J. Zubieta. *Inorg. Chim. Acta*, **250**, 303 (1996).
[22] Z.G. Han, Y.L. Zhao, J. Peng, H.Y. Ma, Q. Liu, E.B. Wang, N.H. Hu. *J. Solid State Chem.*, **177**, 4325 (2004).
[23] C.M. Liu, D.Q. Zhang, D.B. Zhu. *Cryst. Growth Des.*, **5**, 1639 (2005).
[24] H.Y. Zhao, Y.H. Xing, Y.Z. Cao, Z.P. Li, D.M. Wei, X.Q. Zeng, M.F. Ge. *J. Mol. Struct.*, **938**, 54 (2009).
[25] A. Sarkar, S. Pal. *Inorg. Chim. Acta*, **361**, 2296 (2008).
[26] G. Grivani, A.D. Khalaji, V. Tahmasebi, K. Gotoh, H. Ishida. *Polyhedron*, **31**, 265 (2012).
[27] Z.P. Li, Y.H. Xing, C.G. Wang, J. Li, Y.Z. Cao, X.Q. Zeng, M.F. Ge, S.Y. Niu. *Z. Anorg. Allg. Chem.*, **635**, 2601 (2009).

[28] H.Y. Zhao, Y.H. Zhang, Y.H. Xing, Z.P. Li, Y.Z. Cao, M.F. Ge, X.Q. Zeng, S.Y. Niu. *Inorg. Chim. Acta*, **362**, 4110 (2009).
[29] C.M. Hartshorn, P.J. Steel. *Aust. J. Chem.*, **48**, 1587 (1995).
[30] E.A. Nudnova, A.S. Potapov, A.I. Khlebnikov, V.D. Ogorodnikov. *Russ. J. Org. Chem.*, **43**, 1698 (2007).
[31] G.M. Sheldrick. *SADABS, Program for Empirical Absorption Correction for Area Detector Data*, University of Göttingen, Göttingen (1996).
[32] G.M. Sheldrick. *SHELXS 97, Program for Crystal Structure Refinement*, University of Göttingen, Göttingen (1997).
[33] B. Baruah, V.O. Golub, C.J. O'Connor, A. Chakravorty. Eur. J. Inorg. Chem., **12**, 2299 (2003).
[34] C. Preiser, J. Loesel, I.D. Brown, M. Kunz, A. Skowron. *Acta Cryst.*, **55**, 698 (1999).
[35] S. Adams. *Acta Cryst.*, **57**, 278 (2001).
[36] F.D. Costa, G. Lubes, M. Rodríguez, V. Lubes. *J. Solution Chem.*, **40**, 106 (2011).
[37] B.J.A. Jeragh, A. El-Dissouky. *Transition Met. Chem.*, **29**, 579 (2004).
[38] Z.P. Li, Y.H. Xing, Y.Z. Cao, X.Q. Zeng, M.F. Ge, S.Y. Niu. *Polyhedron*, **28**, 865 (2009).
[39] C.J. Ballhausen, H.B. Gray. *Inorg. Chem.*, **1**, 111 (1962).
[40] H.Y. Zhao, F.Y. Bai, Y.H. Xing, Z.P. Li, Y.Z. Cao, X.Q. Zeng, M.F. Ge. *J. Coord. Chem.*, **63**, 435 (2010).
[41] A.W. Addison, T.N. Rao, J. Reedijk, J.V. Rijn, G.C. Verschoor. *J. Chem. Soc., Dalton Trans.*, 13 (1984).
[42] B.S. Parajón-Costa, O.E. Piro, R. Pis-Diez, E.E. Castellano, A.C. González-Baró. *Polyhedron*, **25**, 2920 (2006).
[43] A.C. Gonzalez-Baró, E.E. Castellano, O.E. Piro, B.S. Parajón-Costa. *Polyhedron*, **24**, 49 (2005).
[44] D.C. Crans, M. Mahroof-Tahir, M.D. Johnson, P.C. Wilkins, L.Q. Yang, K. Robbins, A. Johnson, J.A. Alfano, M.E. Godzala, L.T. Austin, G.R. Willsky. *Inorg. Chim. Acta*, **356**, 365 (2003).
[45] R.E. Drew, W.B. Einstein. *Inorg. Chem.*, **12**, 829 (1973).
[46] K. Kanamori, K. Nishida, N. Miyata, K. Okamoto, Y. Miyoshi, A. Tamura, H. Sakurai. *J. Inorg. Biochem.*, **86**, 649 (2001).
[47] Y.H. Xing, K. Aoki, F.Y. Bai. *J. Coord. Chem.*, **57**, 157 (2004).
[48] R.I. de la Rosa, M.J. Clague, A. Butler. *J. Am. Chem. Soc.*, **114**, 760 (1992).
[49] M.R. Maurya, S. Agarwal, C. Bader, M. Ebel, D. Rehder. *Dalton Trans.*, **3**, 537 (2005).
[50] M.R. Maurya, A. Kumar, M. Ebel, D. Rehder. *Inorg. Chem.*, **45**, 5924 (2006).
[51] T.N. Mandal, S. Roy, A.K. Barik, S. Gupta, R.J. Butcher, S.K. Kar. *Polyhedron*, **27**, 3267 (2008).
[52] A. Pohlmann, S. Nica, T.K.K. Luong, W. Plass. *Inorg. Chem. Commun.*, **8**, 289 (2005).
[53] Y.Z. Cao, Z.P. Li, Y.H. Xing, D.M. Wei, Z.F. Pu, M.F. Ge, Z. Shi. *Chem. J. Chin. Univ.*, **32**, 1025 (2011).
[54] D.X. Ren, Y.Z. Cao, C. Chen, Y.H. Xing. *Chem. Res. Chin. Univ.*, **28**, 1 (2012).